Cdc42 GEF Tuba regulates the junctional configuration of simple epithelial cells

Tetsuhisa Otani,[1,2] Tetsuo Ichii,[1,2] Shinya Aono,[1] and Masatoshi Takeichi[1,2]

[1]Graduate School of Biostudies, Kyoto University, Yoshida-Honmachi, Sakyo-ku, Kyoto 606-8501, Japan
[2]RIKEN Center for Developmental Biology, Chuo-ku, Kobe 650-0047, Japan

Epithelial cells are typically arranged in a honeycomb-like pattern, minimizing their cell–cell contact areas, which suggests that some tension operates for shaping of the cell boundaries. However, the molecular mechanisms that generate such tension remain unknown. We found that Tuba, which is a Cdc42-specific GEF, was concentrated at the apical-most region of cell junctions in simple epithelia via its interaction with ZO-1. RNAi–mediated depletion of Tuba altered the geometrical configuration of cell junctions, resulting in a curved and slack appearance. At the subcellular level, Tuba inactivation modified the assembly pattern of junctional F-actin and E-cadherin. Tuba RNAi also retarded cell junction formation in calcium-switch experiments. Suppression of Cdc42 activity or depletion of N-WASP, which is an effector of Cdc42, mimicked the effects of Tuba depletion. Conversely, overexpression of dominant-active Cdc42 or N-WASP enhanced the junction formation of Tuba-depleted cells. These results suggest that Tuba controls the shaping of cell junctions through the local activation of Cdc42 and its effectors.

Introduction

Elucidation of the mechanisms controlling the shape of cells is an important cell-biological issue. In epithelial layers, cells are arranged in an orderly honeycomb-like pattern, in which cell–cell boundaries exhibit a more or less stretched morphology that is similar to the interfaces of soap bubbles, implying that some physical tension is operating for the shaping of cell outlines (Thompson, 1917; Hayashi and Carthew, 2004). The molecular mechanisms that produce such tension, however, remain unresolved. In *Drosophila melanogaster* retinal cells, cadherin cell-adhesion molecules were shown to be required for minimizing the surface areas of the cells in contact with each other (Hayashi and Carthew, 2004), suggesting that this molecular family controls the tensile property of cell junctions. Cadherin organizes the complex machinery for cell adhesion by interacting with several cytoplasmic components, including catenins. This complex is concentrated at the adherens junction (AJ), which is located directly under the tight junction (TJ; Farquhar and Palade, 1963), and these two types of junctional structures are positioned at the apical-most margin of the entire cell–cell junction, although the cadherin–catenin complex is also distributed throughout the lateral cell–cell contacts. The AJ is lined with actin fibers, and cadherin requires α-catenin, which is one of the catenins that is known to interact with F-actin (Rimm et al., 1995; Drees et al., 2005; Yamada et al., 2005), for its full adhesive activity (Watabe-Uchida et al., 1998), suggesting that cadherin and F-actin cooperate in cell junction organization. In turn, regulators of cadherin or actin are assumed to be involved in the modulation of cell–cell boundary morphology.

Rho family small GTPases (Rho GTPases) are pivotal regulators of the actin cytoskeleton (Etienne-Manneville and Hall, 2002). In epithelial cells, these GTPases have also been implicated in cadherin activities (Fukata and Kaibuchi, 2001; Braga and Yap, 2005); conversely, the GTPase activities are modulated by cadherin-mediated adhesion (Kim et al., 2000; Noren et al., 2001; Braga and Yap, 2005), suggesting that these enzymes are important for cadherin–actin interplay. The activities of Rho GTPases are regulated by guanine nucleotide exchange factor (GEF), which exchanges GDP for GTP (Schmidt and Hall, 2002). Once activated, the small GTPases can interact with various downstream effectors, acting as a molecular switch (Etienne-Manneville and Hall, 2002). Among several classes of protein identified as Rho GEFs, the Dbl family proteins are best characterized. The Dbl homology domain (DH domain) has

Correspondence to Masatoshi Takeichi: takeichi@cdb.riken.jp

S. Aono's present address is the Institute for Frontier Medical Sciences, Kyoto University, Sakyo-ku, Kyoto 606-8507, Japan.

Abbreviations used in this paper: AJ, adherens junction; DH, Dbl homology; GEF, guanine nucleotide exchange factor; MLC, myosin light chain; N-WASP, neural Wiskott-Aldrich syndrome protein; TJ, tight junction.

The online version of this article contains supplemental material.

The Journal of Cell Biology, Vol. 175, No. 1, October 9, 2006 135–146
http://www.jcb.org/cgi/doi/10.1083/jcb.200605012

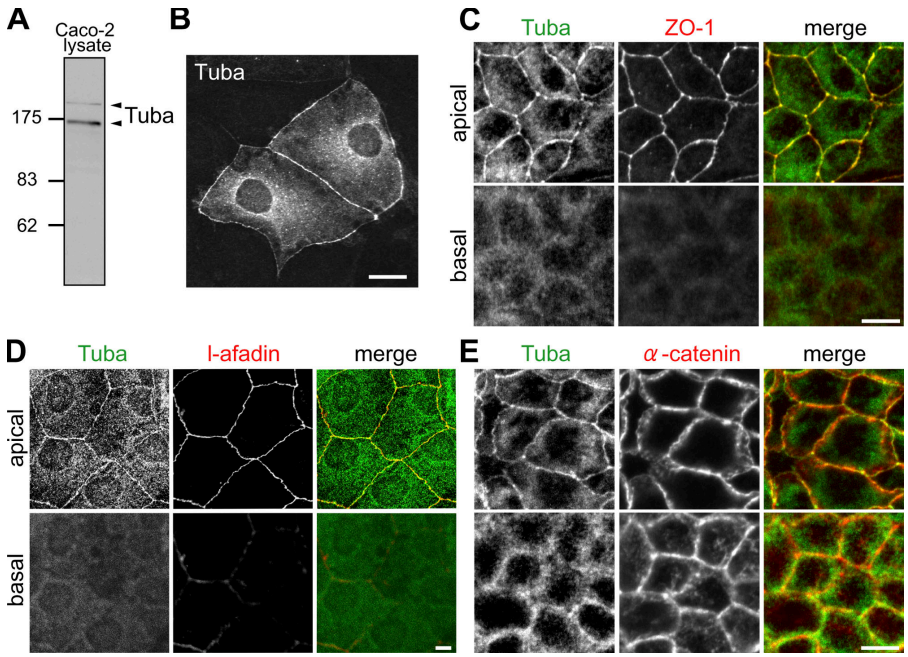

Figure 1. **Localization of Tuba at the apical cell–cell junctions in Caco-2 cells.** (A) Immunoblot detection of Tuba from a Caco-2 cell lysate with anti-Tuba mAb. Two isoforms, of 190 and 170 kD, are detected. (B) Cell junctional signals of Tuba are increased by its exogenous expression. Compare the immunofluorescence signals along cell junctions between the centrally located transfectants and surrounding nontransfectants. (C–E) Endogenous Tuba is concentrated at the apical region of cell junctions. Cells were coimmunostained for Tuba and ZO-1 (C), l-afadin (D), or αE-catenin (α-catenin) (E). Tuba is colocalized with ZO-1, l-afadin, and the apical-most population of αE-catenin (α-catenin). Bars: (B) 20 μm; (C–E) 10 μm.

been shown to be necessary and sufficient for the GEF activity of Dbl family Rho GEFs (Hart et al., 1994). It is thought that localized activation of GEFs contributes to the spatiotemporal activation of Rho GTPases. Among the Rho GEFs identified, Tiam1, which is a Rac-specific GEF, has been best characterized as a modulator of cell junctions, and its depletion impairs both AJ and TJ formation (Malliri et al., 2004; Chen and Macara, 2005; Mertens et al., 2005). GEF-H1/Lfc, which is a GEF for Rho, was also implicated in TJ functions (Benais-Pont et al., 2003). On the other hand, the role of Cdc42 and its GEFs in cell junction assembly is poorly understood, although the activation of Cdc42 was shown to increase actin accumulation at cell junctions (Kodama et al., 1999). Also, nectin, which is an AJ component, could activate Cdc42 through FRG, which is a Cdc42 GEF (Fukuhara et al., 2004). We show that Tuba, which is a Cdc42-specific GEF that belongs to the Dbl family (Salazar et al., 2003), plays an important role in the regulation of cell junction configuration by becoming localized at the apical junctions of simple epithelia.

Results

Tuba localizes at the apical junction by interacting with ZO-1

We used Caco-2 cells throughout the present experiments, as they exhibited typical simple epithelial morphology. Immunostaining with a mAb specific for Tuba (Fig. 1 A) showed that this molecule was sharply concentrated at cell junctions (Fig. 1, C–E). When Tuba cDNA had been introduced into Caco-2 cells, the intensity of junctional Tuba signals increased (Fig. 1 B), justifying the aforementioned observation on the endogenous Tuba localization. A similar distribution was observed in other simple epithelial cells, such as DLD-1 and MTD-1A (unpublished data). Immunostaining of Caco-2 cells at high densities showed that Tuba was strictly localized at the apical-most margin of cell junctions, colocalizing with ZO-1, which is a TJ component (Fig. 1 C). Tuba also colocalized with l-afadin (Mandai et al., 1997), which is an AJ component (Fig. 1 D). However, although the l-afadin was also detectable at basal regions of the cell–cell contacts, to some extent, Tuba did not follow this localization of l-afadin. Tuba also overlapped with the apical margin population of αE-catenin, although the latter was distributed throughout the cell–cell contacts (Fig. 1 E). Other populations of Tuba molecules were localized in the cytoplasm, which were most abundant at perinuclear regions.

Because Tuba closely colocalized with ZO-1, we investigated their potential interactions. First, we observed the localization of these molecules in low-calcium medium, in which cadherin molecules became dispersed but ZO-1 remained as clusters. Even under these conditions, Tuba maintained its colocalization with ZO-1 (Fig. 2 A). We then overexpressed Tuba and ZO-1 together in Caco-2 cells. Excessive Tuba molecules were localized not only along cell junctions, but also became clustered in the cytoplasm, and ZO-1 tightly associated with all these Tuba signals (Fig. 2 B). As a control, we coexpressed Tuba and β-catenin, but these two molecules did not colocalize (Fig. 2 C), indicating that the Tuba–ZO-1 colocalization was caused by their specific interactions.

We next performed immunoprecipitation using lysates of cells cotransfected with Tuba and ZO-1 cDNAs and found that Tuba coprecipitated with ZO-1 (Fig. 2 D). Tuba was also able to coprecipitate with ZO-2, but not with ZO-3 (Fig. S1, A and B, available at http://www.jcb.org/cgi/content/full/jcb.200605012/DC1). To determine the sites on Tuba responsible for its interaction with ZO-1, we coexpressed a series of deletion mutants of Tuba with ZO-1, tested their binding by immunoprecipitation, and found that their interaction required the C-terminal domain of Tuba (Fig. 2, E and F). However, the C-terminal fragment alone was unable to bind ZO-1 (unpublished data), suggesting that some cooperation of the C-terminus with other sites on

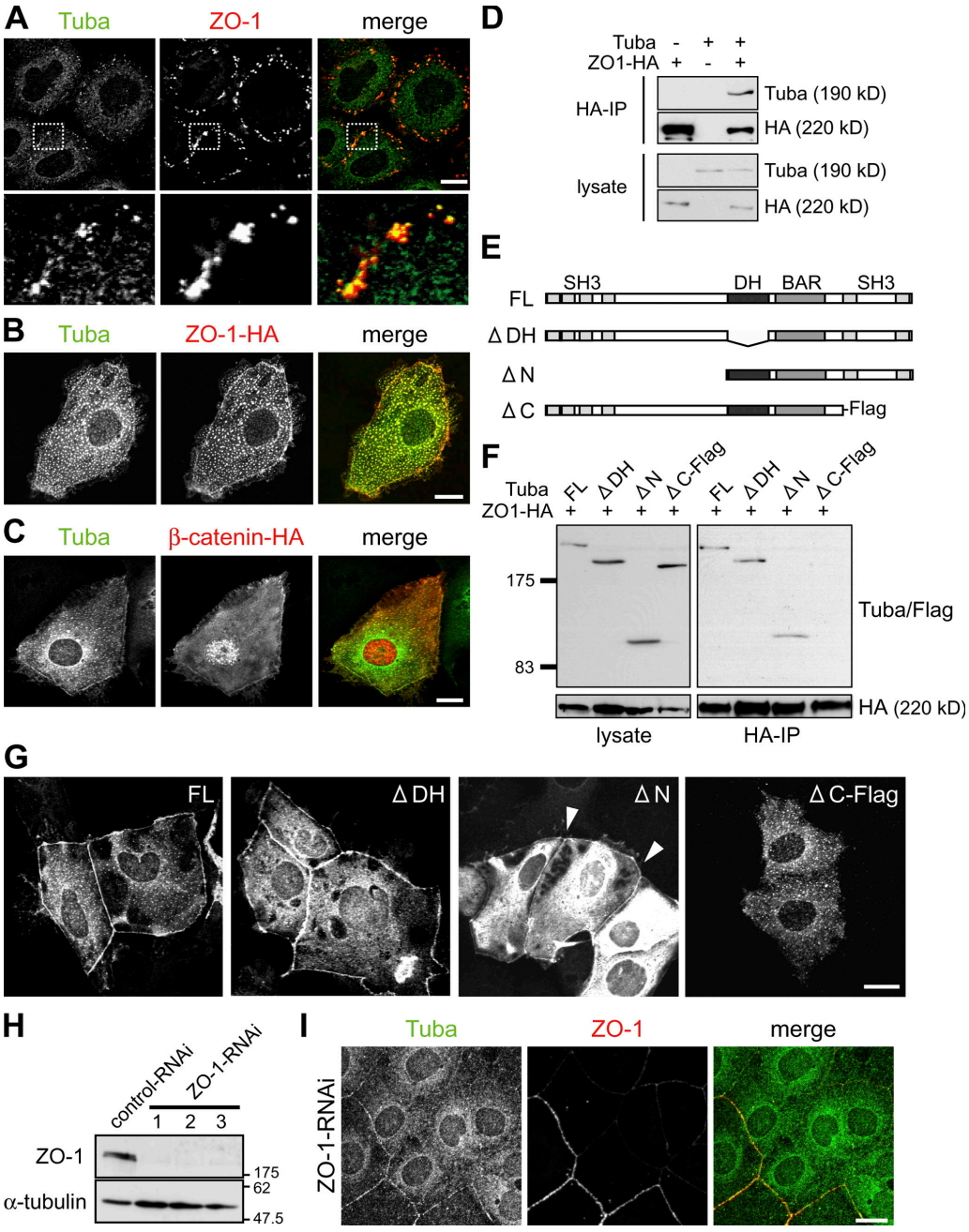

Figure 2. **Tuba is recruited to cell–cell junctions with ZO-1.** (A) Tuba and ZO-1 are colocalized with each other even after disorganization of cell–cell contacts. Caco-2 cells were cultured in low-calcium medium and coimmunostained for Tuba and ZO-1. (B and C) Clusters of overexpressed Tuba are colocalized with ZO-1 (B), but not with β-catenin (C). (D) Tuba coimmunoprecipitates with ZO-1. Tuba and ZO-1-HA were coexpressed in human embryonic kidney 293 cells; and ZO-1 was immunoprecipitated from their lysates with anti-HA antibody, and then the coprecipitated molecules were identified by immunoblotting. (E) Schematic diagram of deletion mutants of Tuba used in this study. From the N-terminus, Tuba consists of four Src homology 3 (SH3) domains, a DH domain, a Bin1/amphiphysin/Rvs (BAR) domain, and two SH3 domains. Flag tag was attached only to ΔC. For immunodetection of Tuba or its mutants, we generally used the anti-Tuba mAb, which had been generated against the C-terminal portion of Tuba. For detection of ΔC, we used anti-Flag antibodies. (F) Tuba C terminus is required for the interaction between Tuba and ZO-1. Deletion mutants of Tuba were coexpressed with ZO-1, and their coprecipitates were assayed as in D. Bands were detected by using a mixture of mAbs against Tuba and Flag tag. (G) Tuba C terminus is required for junctional localization. FL, ΔDH, and ΔN are localized at cell junctions (arrowheads), as well as in the cytoplasm, whereas ΔC is detected only in the cytoplasm. (H and I) Junction localization of Tuba is abolished in ZO-1 knockdown cells. Expression of ZO-1 was knocked down in Caco-2 cells by siRNA (H). ZO-1 RNAi cells were coimmunostained for Tuba and ZO-1 (I). Similar results were obtained by using three different siRNAs, siZO-1-1–3. Bars, 20 μm.

Tuba may be required for the Tuba–ZO-1 interaction. The importance of the C-terminal domain was confirmed by immunostaining of Tuba deletion-mutant transfectants (Fig. 2 G). Constructs in which the DH or N-terminal half region had been deleted, designated as ΔDH or ΔN, respectively, could become localized at cell junctions, although ΔN was largely cytoplasmic. In contrast, ΔC was completely cytoplasmic. Finally, we depleted ZO-1 expression by using RNAi, and

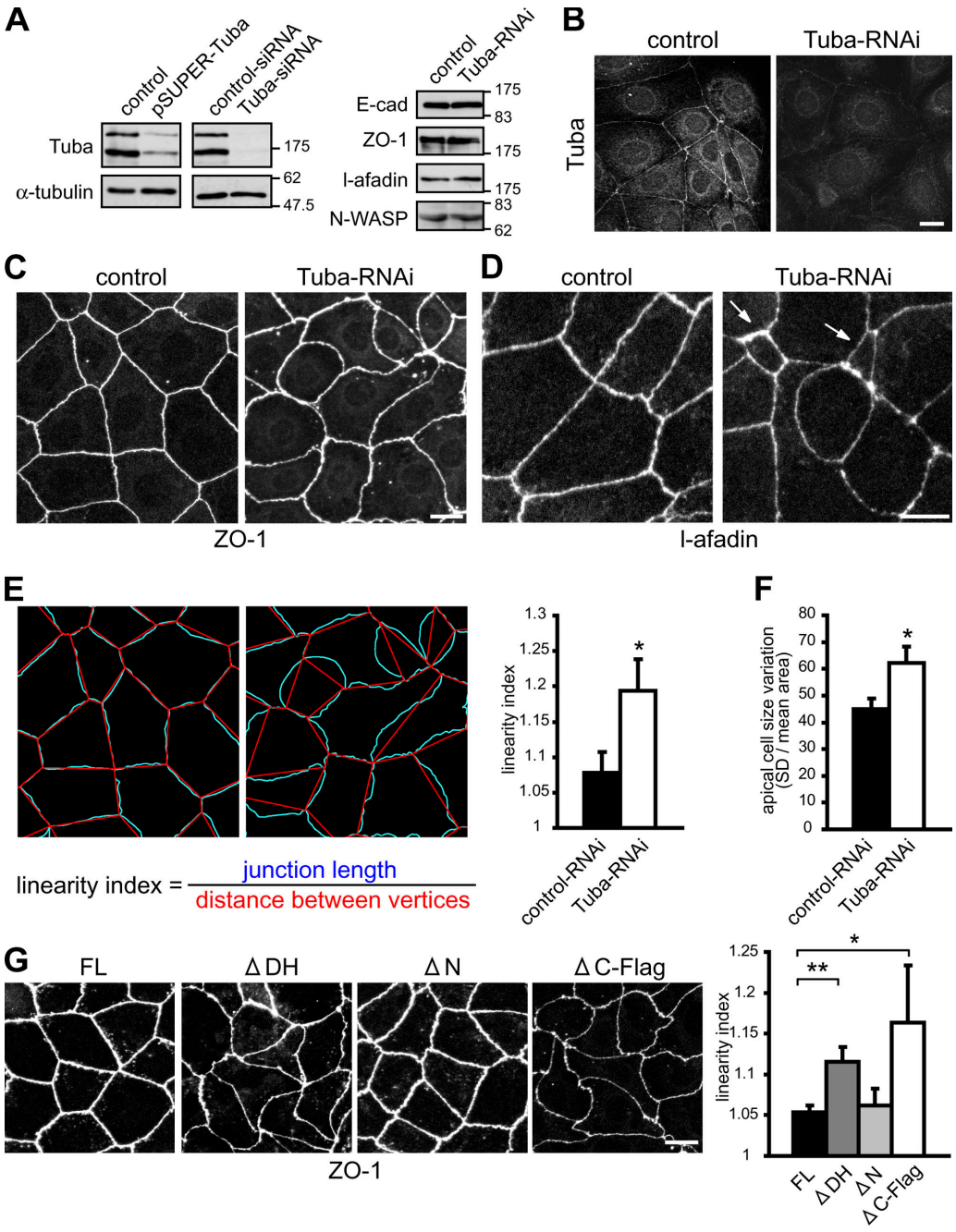

Figure 3. **Tuba regulates the junctional configuration.** (A) Immunoblot detection of Tuba from control, pSUPER-Tuba–transfected, and Tuba siRNA–treated cells by use of anti-Tuba mAb. (B) Immunostaining of control and pSUPER-Tuba–transfected cells with anti-Tuba mAb. (C and D) Distorted apical junctions in Tuba-RNAi cells. Control and Tuba-RNAi cells were stained for ZO-1 (C) or l-afadin (D). In Tuba-RNAi cells, the apical junctions are more irregularly curved than in the controls. Some cells exhibit abnormally small apical surface areas, as outlined by these markers (arrows). (E) Quantification of junction linearity. Junction length (blue) and the distance between vertices (red) were measured. Linearity index is defined by the ratio of junction length to the distance between vertices. (right) This index increases in Tuba-RNAi cells. *, $P < 0.05$. $n = 3$ independent experiments, in each of which >150 junctions were measured; *t* test. (F) Apical area is more variable in Tuba-RNAi cells. The apical area of each cell was measured, and the ratio of the SD of apical area to mean apical area was quantified. *, $P < 0.05$; $n = 3$ independent experiments, in each of which >100 cells were measured; *t* test. (G) Cell junction outlines are distorted in ΔDH- or ΔC-expressing cells, but not in FL- or ΔN-expressing ones. Stable transfectants were immunostained for ZO-1. (right) Quantification confirms these differences. Error bars represent the mean ± the SD. *, $P < 0.05$; **, $P < 0.001$. $n = 4$ independent experiments, in each of which >30 junctions were measured; *t* test. Bars, 20 μm.

found that Tuba could not become localized at the cell junctions that had lost ZO-1 (Fig. 2, H and I), despite the normal appearance of the apical junctions in ZO-1–deficient cells (McNeil et al., 2006; Umeda et al., 2004). These results confirmed that ZO-1 was required for the cell junction localization of Tuba. On the other hand, ZO-2 depletion did not affect Tuba localization (Fig. S1 C), indicating that ZO-1 plays the predominant role in targeting Tuba to cell junctions. Whether Tuba directly binds ZO-1 or -2 or requires a mediator remains to be determined.

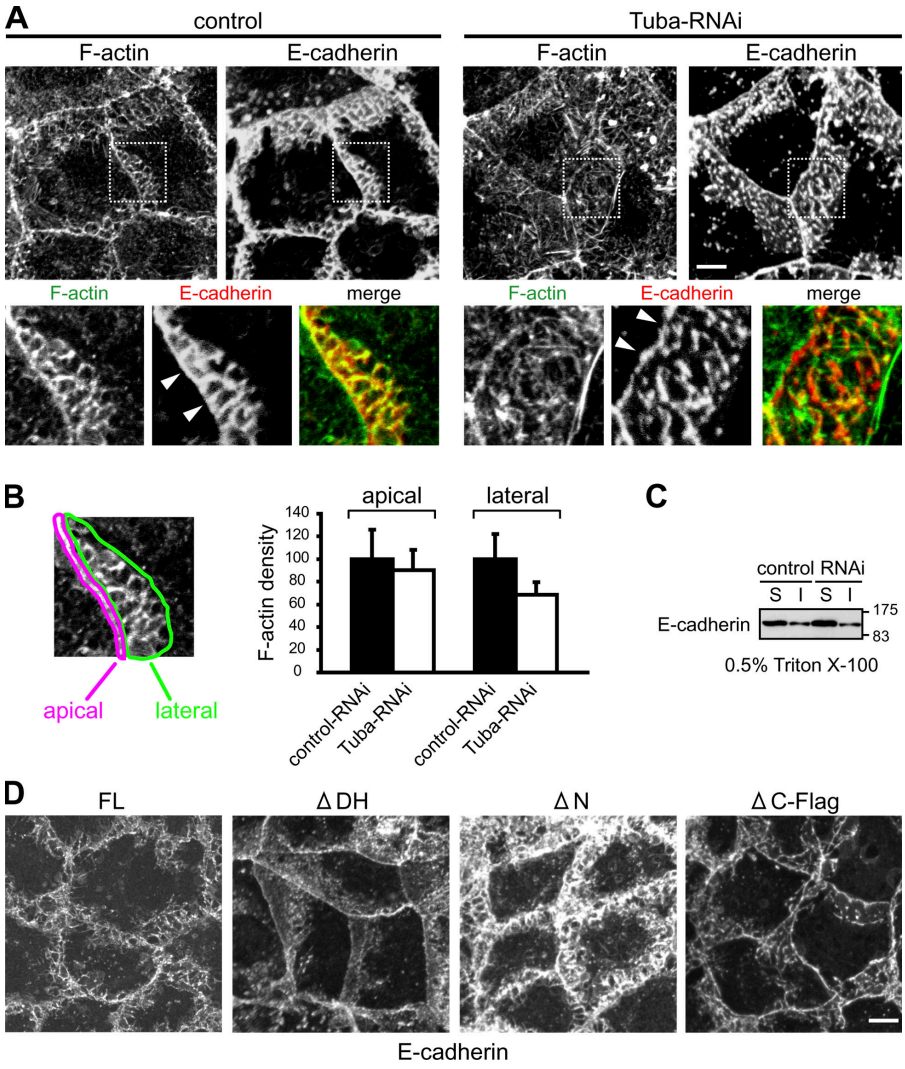

Figure 4. **Disorganization of F-actin and E-cadherin networks by Tuba suppression.** (A) Double-staining for F-actin (green) and E-cadherin (red). F-actin and E-cadherin form an AJ at the apical-most margin of the junction (arrowheads), and the AJ is linked with the lateral networks of these molecules in the case of control cells. In Tuba-RNAi cells, F-actin appears to have been dispersed at the lateral portions, and the E-cadherin networks have become fragmented and discontinuous with the AJ; the colocalization of E-cadherin and F-actin is also reduced. (B) Quantification of F-actin density at cell junctions. (left) F-actin density at apical and lateral cell junctions was measured as shown. (right) Quantification shows that lateral F-actin density is reduced in Tuba-RNAi cells. Error bars represent the mean ± the SD. $n > 40$ junctions. (C) Triton X-100 solubility of E-cadherin is not altered in Tuba-RNAi cells. S, soluble fraction; I, insoluble fraction. (D) Effects of Tuba deletion mutants on E-cadherin distribution. Immunostaining for E-cadherin shows that, in ΔDH- or ΔC-expressing cells, E-cadherin localization at lateral cell–cell contacts is more diffuse compared with that in FL-expressing cells. In ΔN-expressing cells, E-cadherin was most highly concentrated at lateral cell–cell contacts. Bars, 10 μm.

Tuba depletion perturbs junctional configuration

To elucidate the function of Tuba in Caco-2 cells, we examined the effect of its RNAi-mediated depletion, either by isolating stable transfectants expressing small hairpin Tuba RNAs or by treating cells with a siRNA specific for Tuba, and the results consistently observed in these transfectants (Tuba-RNAi cells) are described in this study. Efficient and specific knockdown of Tuba was confirmed by Western blotting and immunofluorescence (Fig. 3, A and B). Immunostaining for ZO-1 and l-afadin revealed that, in Tuba-RNAi cells, the overall outlines of TJ and AJ were distorted; their cell–cell boundaries were overly bent and less strained, compared with those in the controls (Fig. 3, C and D), suggesting that those junctions had acquired reduced tension. We quantified this difference by measuring the ratio of junction length to the distance between vertices, defining a "linearity index," and confirmed that the junctions of Tuba-RNAi cells were excessively curved (Fig. 3 E). Concomitantly, some of the Tuba-RNAi cells exhibited unusually small apical areas (Fig. 3 D, arrows). Quantification showed that the variation in the apical surface area increased after Tuba depletion (Fig. 3 F).

We also tested the effects of overexpression of Tuba deletion mutants in Caco-2 cells (Fig. 3 G). ΔDH lacking the catalytic domain perturbed the junction linearity, as found in Tuba RNAi cells, and ΔC expression showed an effect similar to that of ΔDH, suggesting that these mutant molecules compete with endogenous Tuba for interactions with partners required for their functions. These results corroborated the observation that Tuba inactivation led to the distortion of junctional morphology.

Impaired distribution of E-cadherin and F-actin after Tuba depletion

Despite the deformed outlines of the apical cell–cell contacts, E-cadherin and F-actin appeared normally concentrated along the AJ in Tuba RNAi cells (Fig. 4 A). The expression levels of E-cadherin and other junctional proteins were also not changed (Fig. 3 A). However, their distributions in lower (lateral) portions of cell–cell boundaries were affected. In normal Caco-2 cells, E-cadherin was concentrated at these areas in a peculiar networklike pattern, overlapping with actin fibers with a similar network (Fig. 4 A). Close-up views showed that the lateral populations of E-cadherin or overlapping F-actin organized strands that were linked with their AJ components. In Tuba-RNAi cells,

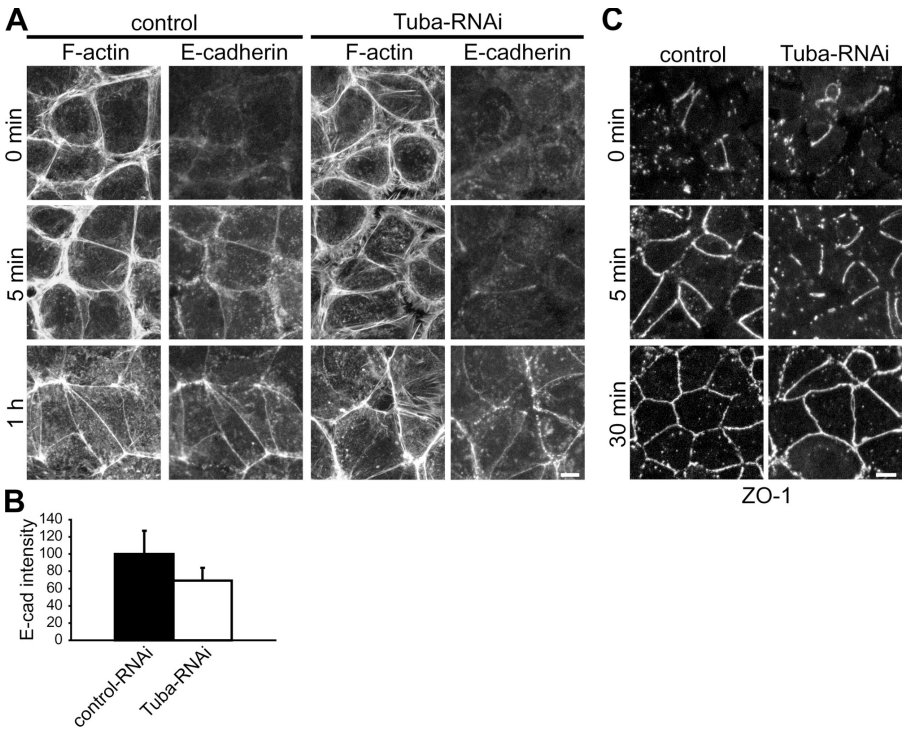

Figure 5. **Junctional recruitment of F-actin and E-cadherin after calcium switch.** (A) Cells were cultured in low-calcium medium overnight, and then cadherin-mediated junction assembly was initiated by the addition of calcium. In Tuba-RNAi cells, the relocation of E-cadherin to cell junctions was retarded, and F-actin could not be reorganized into sharp lines at cell–cell boundaries by 1 h. (B) Immunofluorescence intensity of E-cadherin at cell junctions was quantified for the samples incubated for 5 min with calcium. Error bars represent the mean ± the SD. $n = 60$ junctions. (C) ZO-1 relocation to cell junctions was not severely effected in Tuba-RNAi cells. Bars, 10 μm.

E-cadherin strands became fragmented and discontinuous with the AJ, with a concomitant disturbance of actin filaments, which appeared less polymerized than in the controls. Quantification of F-actin density at cell junctions confirmed that the lateral actin fibers less densely distributed in the RNAi cells, although the apical actin filaments were only slightly affected (Fig. 4 B). In addition, Tuba depletion reduced the colocalization of E-cadherin and actin fibers, although the Triton X-100 solubility of E-cadherin was not particularly different between control- and Tuba-RNAi cells (Fig. 4 C).

We also generated stable transfectants expressing Tuba deletion mutants, and examined E-cadherin distribution in them (Fig. 4 D). In ΔDH- and ΔC-expressing cells, E-cadherin at the lateral membranes appeared more diffuse or fragmentary, as compared with that of FL-expressing cells. Thus, these two constructs not only impaired apical junctional linearity (see above) but also perturbed the lateral distribution of E-cadherin, as in the case of Tuba-depleted cells. On the other hand, in ΔN-expressing cells, E-cadherin became more highly concentrated at the cell–cell contacts. This implies that the N-terminal half region has an inhibitory activity for Tuba.

To see the effects of Tuba depletion on more dynamic phases of cell contact, we observed the behavior of E-cadherin and F-actin during the recovery process of cell–cell adhesion by conducting a "calcium-switch" experiment (Fig. 5 A). In low-calcium medium, E-cadherin disappeared from cell–cell boundaries, and actin fibers irregularly ran along cell peripheries in both control and Tuba-RNAi cells. By 1 h after calcium restoration, E-cadherin and actin became sharply colocalized at cell–cell boundaries. In Tuba-RNAi cells, however, this E-cadherin accumulation was retarded. At 1 h, although we could detect junctional E-cadherin, its signals were fragmented, and actin fibers did not sharply delineate cell–cell boundaries. Furthermore, E-cadherin signals did not fully colocalize with F-actin ones. The retardation of E-cadherin accumulation was confirmed by quantifying the junctional fluorescence intensity of E-cadherin at 5 min after calcium switch (Fig. 5 B). In contrast to E-cadherin, ZO-1 recruitment to cell junctions was not severely affected in Tuba-RNAi cells (Fig. 5 C), although the outlines of these cells appeared to be less tense compared with those of control cells. These results suggest that the junctional recruitment of ZO-1 occurs independently of the Tuba signaling, whereas the organization of E-cadherin and actin at cell junctions is under the control of Tuba. Meanwhile, we found no difference in the composition of catenins coprecipitating with E-cadherin between the control and Tuba-RNAi cell lysates (unpublished data), indicating that Tuba deficiency did not affect cadherin–catenin complex formation.

The effects of ZO-1 knockdown on junctional configuration

As ZO-1 knockdown depleted Tuba from cell junctions, we expected that ZO-1–RNAi and Tuba-RNAi cells would display similar phenotypes. However, this was not the case. The outlines of apical junctions appeared rather straighter in ZO-1–RNAi cells than in the controls (Fig. S2 A, available at http://www.jcb.org/cgi/content/full/jcb.200605012/DC1), which is opposite to what we had anticipated. We noticed that myosin IIA or IIB became strongly up-regulated along the apical junctions of ZO-1–depleted cells (Fig. S2 B); furthermore, phosphorylation of serine 19 of myosin light chain (MLC), which reflects its activation, was also up-regulated at ZO-1–depleted cell junctions (Fig. S2 C). In Tuba-RNAi cells, on the other hand, neither myosin localization nor MLC phosphorylation was up-regulated

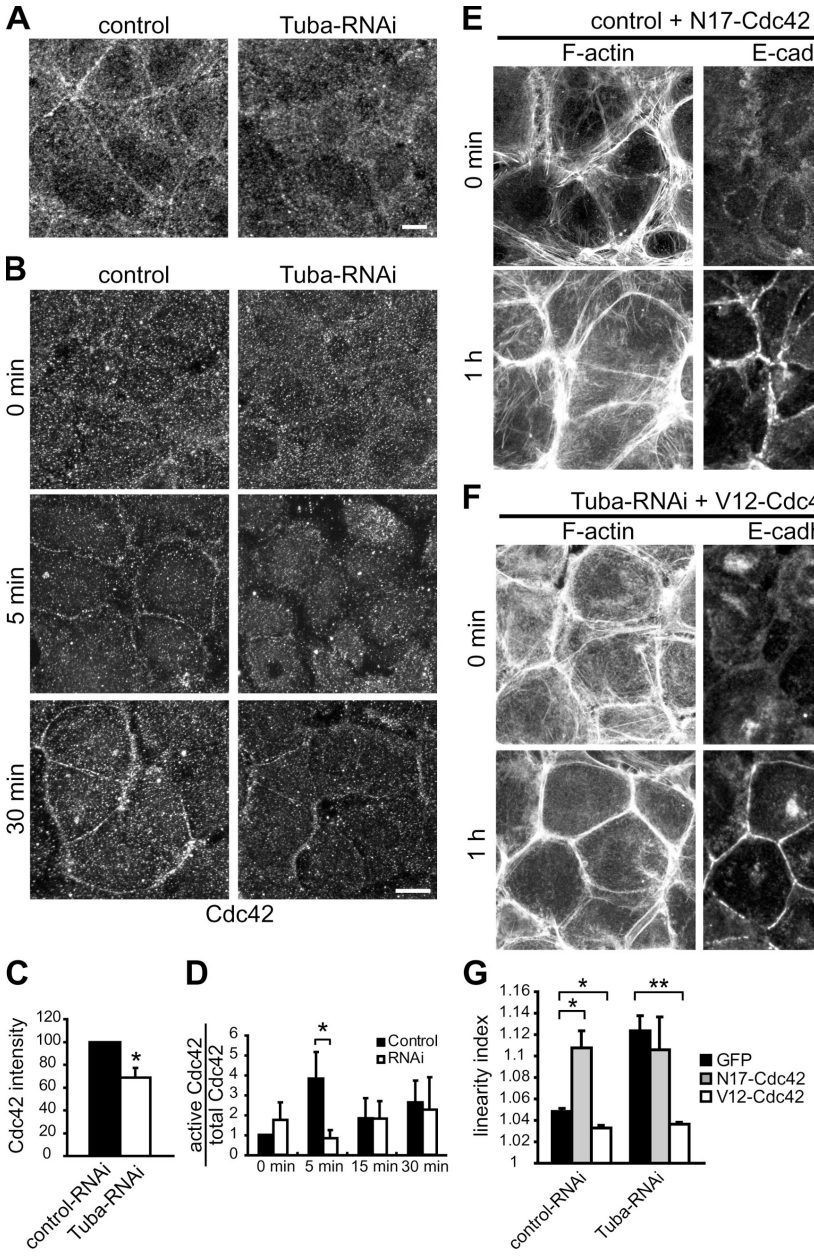

Figure 6. **Role of Cdc42 in junction assembly.** (A) Cdc42 is localized at cell–cell boundaries, and this localization is diminished in Tuba-RNAi cells. (B and C) Delayed redistribution of Cdc42 to Tuba-RNAi cell junctions in calcium-switch experiments. Cdc42 was immunostained at the indicated times after calcium restoration (B). Immunofluorescence intensity of Cdc42 at cell junctions was quantified for the samples incubated for 30 min (C), in which the intensity of control-RNAi cells was adjusted to 100. Error bars represent the mean ± the SD. *, $P < 0.05$. $n = 3$ independent experiments, in each of which >10 junctions were measured; paired *t* test. (D) Delayed activation of Cdc42 in Tuba-RNAi cells. After Cdc42 pull-down assays using GST-PAK-CRIB, the intensity of electrophoretic bands of Cdc42 was quantified. In brief, each band was encircled by a box, and the signal density of the band was measured. The ratio of the Cdc42 signals in GST-PAK-CRIB pull-down samples to those in the total lysates was defined as "active Cdc42/total Cdc42." The ratio in control-RNAi cells at 0 min was adjusted to 1. Error bars represent the mean ± the SEM. *, $P < 0.05$; $n = 3$ independent experiments; one-tailed *t* test. (E and F) Effects of Cdc42 mutants on junction assembly in calcium-switch assays. Dominant-negative (N17-Cdc42) or constitutive-active (V12-Cdc42) Cdc42 was expressed in control or in Tuba-RNAi cells. In N17-Cdc42–transfected control cells (E), the junctional recruitment of F-actin and E-cadherin was delayed (compare with Fig. 5). (F) In contrast, V12-Cdc42 strongly promoted the junctional accumulation of these molecules in Tuba-RNAi cells. (G) Linearity index in control or Tuba-RNAi cells, expressing either GFP (control) or dominant-negative or constitutive-active Cdc42, measured at 1 h. Error bars represent the mean ± the SD. *, $P < 0.005$; **, $P < 0.0005$. $n = 3$ independent experiments, in each of which >40 junctions were measured; *t* test. Bars: (A) 10 μm; (B, E, and F) 20 μm.

at cell junctions (Fig. S2, E and F). From these observations, we reasoned that ZO-1 depletion up-regulated myosin II activities via unknown mechanisms, and enhanced the contractility of junctional actin fibers, hiding the opposite effect of Tuba depletion. To test this possibility, we examined the effect of Y-27632, which is an inhibitor of Rho kinase (Uehata et al., 1997) that can suppress MLC activation (Amano et al., 1996), and found that this reagent abolished the up-regulation of myosin II in ZO-1–RNAi cells (Fig. S2 D). Importantly, in the presence of Y-27632, the cell junctions now became more severely distorted in ZO-1–RNAi cells than in the controls (Fig. S2 A), indicating that, provided myosin II is inactive, ZO-1 and Tuba depletions exhibit similar junctional phenotypes. These findings suggest that there are at least two pathways downstream of ZO-1, a Rho–Rho kinase–myosin pathway and a Tuba pathway, and that ZO-1 depletion affected both pathways. As Y-27632 alone can distort cell junctions to some extent (Fig. S2 A), a balance between these pathways may determine the overall junction morphology. Collectively, we can conclude that the phenotypes observed in ZO-1–depleted cells do not contradict with the proposed role of the interaction between ZO-1 and Tuba in cell junction configuration. It is of note that cell junction formation is delayed in ZO-1–depleted cells (McNeil et al., 2006; Umeda et al., 2004), which is similar to the properties of Tuba-RNAi cells, supporting the idea that ZO-1–dependent localization of Tuba at cell junctions is required for its functions.

Tuba signals through Cdc42

Next, we studied the functions of Tuba as a Cdc42 GEF. We first confirmed that Tuba preferentially activated Cdc42 by conducting an in vitro guanine nucleotide exchange assay (Fig. S3, available at http://www.jcb.org/cgi/content/full/jcb.200605012/DC1).

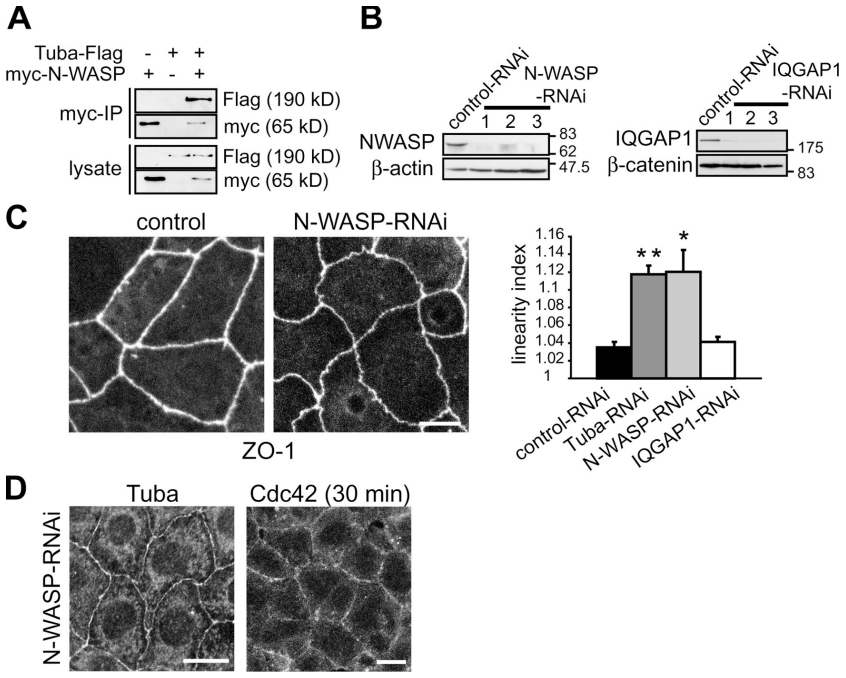

Figure 7. **Role of N-WASP in junctional configuration.** (A) Tuba interacts with N-WASP. Tuba and myc-N-WASP were coexpressed in human embryonic kidney 293 cells, N-WASP was immunoprecipitated from their lysates with anti-myc antibody, and the coprecipitated molecules were identified by immunoblotting. (B, left) Immunoblot detection of N-WASP from control and N-WASP–RNAi cells with anti–N-WASP antibody. (right) Immunoblot detection of IQGAP1 from control and IQGAP1-RNAi cells with anti-IQGAP1 antibody. (C) Distortion of cell–cell boundaries in N-WASP–RNAi cells, detected by ZO-1 immunostaining. (right) Linearity index. Error bars represent the mean ± the SD. *, $P < 0.005$. **, $P < 0.0005$. $n = 3$ independent experiments, in each of which >100 junctions were measured; *t* test. (D) Localization of Tuba and Cdc42 is not altered in N-WASP–RNAi cells. (left) Tuba localization in confluent N-WASP–RNAi cells. (right) Cdc42 localization in N-WASP–RNAi cells at 30 min after calcium restoration. Bars, 20 μm.

As the activation of Rho GTPases has been correlated with its membrane association (Bokoch et al., 1994), we examined the subcellular localization of Cdc42 in Caco-2 cells by immunostaining. In confluent Caco-2 cells, immunostaining signals for Cdc42 were weakly, but consistently, detected at the apical cell–cell junctions, and this localization of Cdc42 became less visible in Tuba-RNAi cells (Fig. 6 A). When cells had been subjected to calcium-switch experiments, Cdc42 was rapidly recruited to cell–cell contact sites upon the restoration of normal calcium concentration in the control cells, and this redistribution of Cdc42 was retarded in the Tuba-RNAi cells (Fig. 6 B). The Cdc42 immunofluorescence signal per cell junction was reduced by ∼30% in the Tuba-RNAi cells, when measured at the 30 min incubation point (Fig. 6 C). These observations suggest that Tuba has the ability to facilitate the recruitment of Cdc42 to cell junctions. Because Cdc42 was shown to be activated during cell junction assembly (Kim et al., 2000; Noren et al., 2001), we measured its activity by pull-down assays. The results showed that Cdc42 was transiently activated at 5 min after calcium switch, but this activation did not occur in Tuba-RNAi cells (Fig. 6 D). We could not detect any other differences in the overall activity of Cdc42 between control and Tuba-RNAi cells by this biochemical method; the Tuba-mediated Cdc42 regulation might represent only a small portion of the entire regulatory systems for this small GTPase.

To test if the cellular phenotypes observed in Tuba-RNAi cells were caused by reduced Cdc42 activities, we examined if dominant-negative Cdc42 expression could mimic Tuba depletion. Caco-2 cells transfected with Cdc42 mutants were unable to grow to form cell colonies, and for this reason, we observed only early cell–cell contact events by using calcium-switch assays. In the cells transfected transiently with dominant-negative N17-Cdc42, E-cadherin and actin accumulation were perturbed in a fashion similar to those found in Tuba-RNAi cells. E-cadherin remained punctate and F-actin irregularly delineated cell junctions at 1 h after the calcium restoration (Fig. 6 E). Conversely, when dominant-active V12-Cdc42 had been expressed in Tuba-RNAi cells, the E-cadherin and actin reassembly was dramatically facilitated, resulting in the formation of junctions with a tightened appearance (Fig. 6 F). Measurement of the junction linearity confirmed that dominant-negative N17-Cdc42 was able to loosen the cell boundaries of the control cells, but could not significantly enhance the phenotype of Tuba-RNAi cells, and dominant-active V12-Cdc42 enhanced the rectilinear organization of cell junctions in both control and Tuba-RNAi cells (Fig. 6 G). Thus, Cdc42 inactivation mimicked that of Tuba, and activation of Cdc42 could rescue the Tuba RNAi phenotypes. The effect of V12-Cdc42 appeared excessive, as it facilitated even the control cell junction formation, reflecting its dominant-active nature.

Previous studies showed that Tuba interacted with neural Wiskott-Aldrich syndrome protein (N-WASP; Salazar et al., 2003). As N-WASP is an effector of Cdc42 (Rohatgi et al., 1999), we studied its potential role in the Tuba–Cdc42 signaling system. We first confirmed that Tuba could coprecipitate with N-WASP (Fig. 7 A). Next, we knocked down N-WASP by using RNAi (Fig. 7 B). In N-WASP–RNAi cells, the outlines of cell junctions became distorted in a pattern comparable to that in Tuba-RNAi cells (Fig. 7 C). For comparison, we also knocked down the expression of IQGAP1, which is another Cdc42 effector implicated in cell junctions (Kuroda et al., 1998; Noritake et al., 2004), and found that IQGAP1 depletion had no effects on the junction linearity (Fig. 7, B and C), suggesting that these effectors have distinct roles. Tuba and Cdc42 were able to localize normally to cell–cell junctions in the N-WASP–depleted cells (Fig. 7 D), suggesting that these molecules function upstream of N-WASP.

We also examined E-cadherin and actin organization in N-WASP–RNAi cells. In them, E-cadherin strands became fragmented at the lateral cell–cell contacts, as seen in Tuba-RNAi

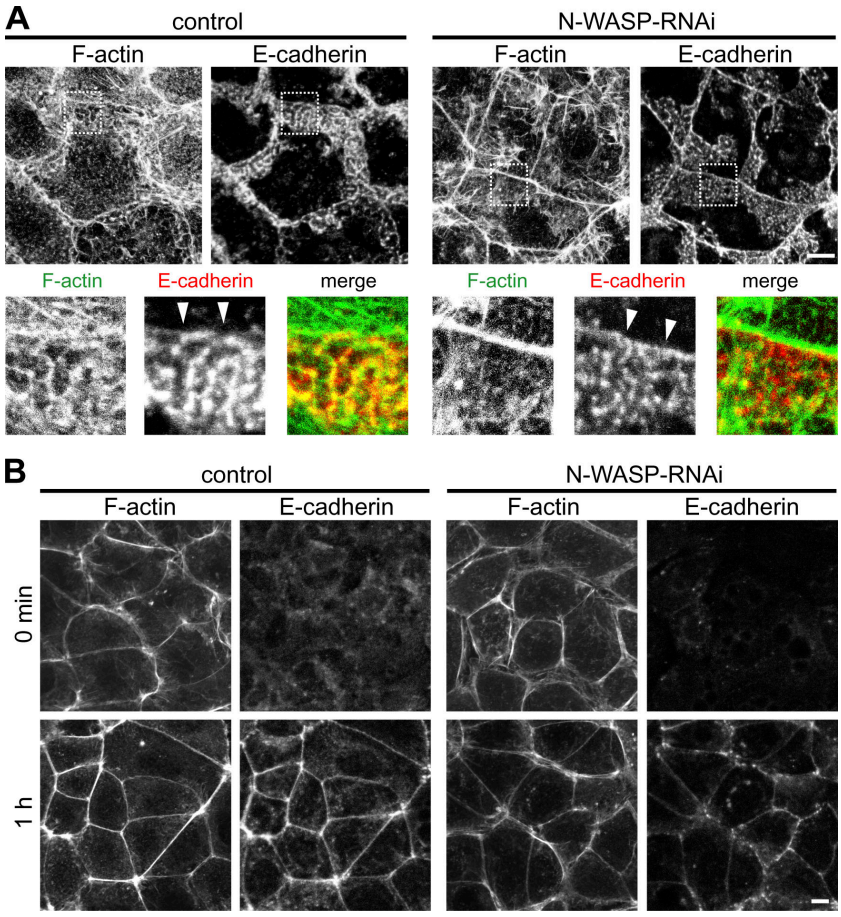

Figure 8. **Role of N-WASP in cadherin or actin distribution.** (A) Double-staining for F-actin (green) and E-cadherin (red) in N-WASP–RNAi cells. Arrowheads indicate the AJ. Note the diffuse actin signals at the lateral cell junctions, and reduced colocalization of F-actin and E-cadherin, in N-WASP–RNAi cells. Actin fibers along the AJ appear normal. (B) Control and N-WASP–RNAi cells were subjected to calcium-switch assays and stained for F-actin or E-cadherin. N-WASP depletion delayed cell junction assembly. Linear reorganization of actin filaments was impaired, and E-cadherin accumulation was irregular at 1 h. Bars, 10 μm.

cells, and their colocalization with F-actin was dramatically reduced (Fig. 8 A). The fibrous organization of actin itself appeared to have been suppressed at the lateral cell–cell contact regions, although the apical AJ-associated bundles were not affected. In calcium-switch assays, N-WASP depletion perturbed the organization of E-cadherin and F-actin at early cell–cell contacts (Fig. 8 B), which is a phenocopy of the effects of Tuba depletion. Finally, by using the calcium-switch assay, we examined whether N-WASP overexpression could rescue the defects of junction assembly that are induced by Tuba depletion. The results showed that overexpression of full-length N-WASP facilitated the accumulation of E-cadherin and F-actin at cell–cell contacts in Tuba RNAi cells (Fig. S4, A and C, available at http://www.jcb.org/cgi/content/full/jcb.200605012/DC1), although this effect was most evident at 5 min after calcium restoration, and became less clear at 1 h. In contrast, overexpression of Δcof-N-WASP, which cannot activate Arp2/3 complex–dependent actin nucleation in vitro (Rohatgi et al., 1999), did not facilitate E-cadherin or F-actin accumulation at cell–cell contacts (Fig. S4, B and D).

Discussion

We have demonstrated that Tuba is concentrated at the apicalmost margin of the epithelial cell junctions by binding to the TJ protein ZO-1 (or its associated proteins), suggesting that this molecule is localized around the TJ. Depletion of Tuba distorted the outlines of the apical TJ–AJ complex. Closer observations of F-actin and E-cadherin revealed that although the AJ structure itself appeared normal, the distributions of these molecules located lower than the AJ were disorganized. In normal Caco-2 cells, F-actin organized a fibrous network at the lateral portions of the cell junction, and this actin network was linked with the apical actin fibers forming the AJ, and E-cadherin showed an overlapping distribution. As a result of Tuba depletion, the E-cadherin networks became fragmented, with a concomitant reduction of thick, lateral actin filaments. These observations suggest a scenario in which Tuba functions at the level of the TJ, but its effects spread to the lower portions of the junction. As such apical-specific localization has never been reported for other Cdc42 or Rac GEFs, Tuba may play a unique, position-specific role in junctional organization.

Our results suggest that Tuba is required for the regulation of geometrical configuration of the apical junctions. Although the mechanism that generates the linear morphology of the apical junctions is poorly understood, we can speculate that the surface tension supported by the cortical actin cytoskeleton is important, as the actin cytoskeleton is a critical regulator of the viscoelasticity of the cell cortex (Petersen et al., 1982). The role of Tuba is likely to regulate actin polymerization via Cdc42 and its effectors, and E-cadherin follows the actin distribution, as suggested by their colocalization. The lateral networks of F-actin and E-cadherin strands, thus formed, may increase the surface tension for minimizing the surface area of cell junctions,

or stabilize the linear morphology of cell junctions, and this molecular status is disrupted by the loss of Tuba. On the other hand, through the experiments of ZO-1 knockdown, we found that ZO-1 functioned not only as a partner for Tuba but also as a regulator of myosin activity, and the latter activity influenced the morphology of cell junctions. In contrast to the case of ZO-1 depletion, Tuba-depletion did not affect myosin distribution or activity, suggesting that actomyosin contractility may not primarily be involved in the loosened appearance of Tuba-depleted cell junctions. It is likely that cooperations of the myosin-dependent contractility and Tuba-mediated actin organization determine the overall shape of cell junctions. As an alternative role of Tuba, it may regulate the dynamics of cadherin molecules, such as their trafficking and endocytosis, thus affecting junction morphology; this possibility remains to be tested in the future.

Supporting the hypothesis that Tuba functions via Cdc42, Tuba promoted recruitment of Cdc42 to cell junctions, transiently activating it during cell junction recovery processes. Dominant-negative and -active Cdc42 mimicked the Tuba depletion and rescued the Tuba RNAi phenotypes, respectively, which is consistent with the idea that Cdc42 acts downstream of Tuba signaling. Furthermore, Tuba was shown to interact with proteins to regulate the actin cytoskeleton, including N-WASP, which is a well-known effector of Cdc42 (Salazar et al., 2003). We demonstrated that N-WASP depletion induced distorted apical junctions, just like Tuba depletion, and also that N-WASP was required for normal accumulation of E-cadherin and F-actin at cell junctions, confirming earlier observations (Ivanov et al., 2005). In addition, N-WASP overexpression restored rapid recruitment of E-cadherin and F-actin to the junctions in Tuba RNAi cells. These results suggest that N-WASP may be one of the components working downstream of the Tuba–Cdc42 pathway; this idea is also supported by a recent study with melanoma cells (Kovacs et al., 2006). N-WASP activates the Arp2/3 complex, which creates branched actin filaments (Blanchoin et al., 2000; Rohatgi et al., 1999); and the Arp2/3 complex was shown to be necessary for cells to assemble cadherin-based cell contacts (Kovacs et al., 2002; Verma et al., 2004). When considering all of the data together, we can imagine a scheme in which N-WASP, activated by Tuba–Cdc42, enhances actin polymerization at the level of the apical junctions. This process then leads to the delivery of polymerized actin filaments to the lower portions of cell junctions, and these actin filaments may serve as a scaffold on which the E-cadherin–catenin complex may be anchored. Although other mechanisms, such as trafficking of E-cadherin might also be involved, this scheme accounts for the putative mechanism as to how Tuba, which is confined to the apical region, can organize F-actin and E-cadherin throughout the lateral cell–cell contacts. Meanwhile, the rescuing effect of N-WASP overexpression on Tuba-depleted cells appeared to have been transient, indicating that other factors are also involved in the Tuba–Cdc42 signaling system.

Calcium-switch experiments showed that Tuba was also required for the initial processes of junction formation. Both E-cadherin and F-actin assemblies were impaired during the reestablishment process of cell–cell contacts. ZO-1 has been shown to form a complex with the cadherin–catenin complex at the early stages of cell junction assembly (Rajasekaran et al., 1996; Ando-Akatsuka et al., 1999), implying that, in nascent cell–cell contacts, Tuba may be in closer proximity to cadherins than in mature junctions, and thus could directly control cadherin-mediated adhesion. Even at early cell–cell contacts, however, cell boundaries always displayed a less-tensed appearance, not only in Tuba-RNAi cells but also in N-WASP–RNAi cells or those expressing dominant-negative Cdc42. These observations suggest that a common function of Tuba governs the initial, as well as the mature, phases of cell–cell contact.

Several GEFs other than Tuba have been implicated in cell–cell adhesion, including Tiam1, which is a Rac-specific GEF (Chen and Macara, 2005; Hordijk et al., 1997), and Asef, which is also a Rac GEF (Kawasaki et al., 2003). FRG participates in nectin-induced activation of Cdc42 (Fukuhara et al., 2004), and GEF-H1 regulates TJ permeability (Benais-Pont et al., 2003). It is likely that many GEFs are sequentially involved in cell junction assembly in a redundant or independent manner. Tiam1 deficiency was reported to disrupt epithelial junctions (Malliri et al., 2004; Mertens et al., 2005). Not only Tuba depletion, but also Tiam1 depletion impairs both AJ and TJ organization. In future studies, it is therefore important to define how Rac and Cdc42 GEFs share their roles in the regulation of cell assembly.

Materials and methods

Plasmid construction

A partial cDNA clone of human Tuba (KIAA1010) was obtained from the Kazusa DNA Institute (Chiba, Japan). The 5′ sequence was determined by 5′-RACE, using a SMART RACE cDNA amplification kit (CLONTECH Laboratories, Inc.), with cDNA from Colo205 cells used as the template. The 5′ fragment was subsequently cloned by RT-PCR. The 40–amino acid deletion in the original KIAA1010 cDNA clone (Salazar et al., 2003) was also amplified by RT-PCR. pSUPER vectors were generated as previously described (Brummelkamp et al., 2002). pGK-neo was further inserted at the EcoRI–NotI site of pSUPER to obtain stable transfectants. The RNAi target sequence of Tuba was designed and inserted into the BglII–HindIII site of pSUPER, as previously described (Brummelkamp et al., 2002). The target sequences were as follows: Tuba-RNAi-1, 5′-AGTCAAGACCTCGTCAAAG-3′; Tuba-RNAi-2, 5′-ACCTTGATGCTCACTAGAA-3′; and cytokeratin 19 (as a specificity control), 5′-GCTAACCATGCAGAACCTC-3′. Stealth siRNAs with the following target sequences were synthesized by Invitrogen: siZO1-1, 5′-GCAGCTCCAAGAGAAATCTTCGAAA-3′; siZO1-2, 5′-GGCAAGAGAAGAACCAGATATTTAT-3′; siZO1-3, 5′-CCCTGGATTTAAGCCAGCCTCTCAA -3′; siZO2-1, 5′- CCCTAAAGGTGAAATGGTGACCATT-3′; siZO2-2, 5′-CCCATAGCTGATATAGCAATGGAAA-3′; siZO2-3, 5′-GGCTAATGAGTTACCTGACTGGTTT -3′; siTuba, 5′-GAGCTTGAGGGAACATACAAGATTT -3′; siNWASP-1, 5′-TCAAATTAGAGAGGGTGCTCAGCTA-3′: siNWASP-2, 5′-TCTGTGGCTGATGGCCAAGAGTCTA-3′; siNWASP-3, 5′-CCCTCTTCACTTTCCTCGGCAAGAA-3′; siIQGAP1-1, 5′-GGCCCTACAGATTCCTGCAGCTAAA -3′; siIQGAP1-2, 5′-GACAGGAAATCCTACGGTTATTAAA -3′; and siIQGAP1-3, 5′-CCAATAAGATGTTTCTGGGAGATAA -3′. Negative-control stealth siRNAs were also obtained from Invitrogen. ΔDH (amino acids 1–734 and 993–1,577), ΔN (amino acids 747–1,577), and ΔC (amino acids 1–1,276) with or without stop codons were generated by PCR and, subsequently, subcloned into the pCA-Sal-Flag-IRES-hygromycin vector to obtain stable transfectants. Mouse ZO-1 cDNA (a gift from S. Tsukita, Kyoto University, Kyoto, Japan) was subcloned in a pCA-Sal-HA vector. The ZO-2 expression vector CAG-NHA-ZO2-Ipuro and ZO-3 expression vector pME18S-ZO3-7myc were also gifts from S. Tsukita. pCA-β-catenin-HA was constructed by K. Tanabe in our laboratory. The N-WASP expression vectors pEF-BOS-myc-N-WASP and pEF-BOS-myc-Δcof-N-WASP were donated by T. Takenawa (University of Tokyo, Tokyo, Japan). Recombinant adenoviruses expressing myc-N17-Cdc42 and myc-V12-Cdc42 were provided by H. Bito and S. Narumiya (Kyoto University, Kyoto, Japan).

Cell culture and transfection

Caco-2 cells were obtained from the American Type Culture Collection. All cell lines were cultured in a 1:1 mixture of DME and Ham's F12 supplemented with 10% FCS. To enhance cell spreading, we cultured the cells on collagen-coated dishes. Cells at 70% confluence were transfected by use of Effectene (QIAGEN), according to the manufacturer's protocol. For siRNA treatments, cells were transfected by the use of Lipofectamine 2000 (Invitrogen), according to the manufacturer's protocol. We obtained >90% reduction in the protein level for all siRNAs at 3–4 d after transfection, and all experiments were performed during this period. Adenovirus infection was performed by incubating cells with a viral solution for 3–6 h. More than 80% of the cells were infected, and the maximal expression of the transgene was observed at 24–48 h after infection, the timeframe in which all experiments were conducted. For isolating stable transfectants, transfected cells were selected by exposure to 400 μg/ml G418 or 100 μg/ml hygromycin. In the case of RNAi-stable lines, the surviving colonies were picked up and cloned, and then examined for the expression of targeted proteins by Western blotting. Multiple clones were isolated for each target sequence, in which >90% knockdown of protein expression was achieved. For the stable transfectants of deletion mutants, the cells were maintained as uncloned populations. For calcium-switch experiments, cells were cultured overnight in calcium-free DME (Invitrogen) supplemented with 10% dialyzed FCS. Cell adhesion was initiated by adding 1.8 mM $CaCl_2$ to the medium. Y-27632 (Calbiochem) was added to cultures at a final concentration of 10 μM, and the cells were fixed after 30 min.

Antibodies

Mouse mAb 5G6 against Tuba was raised by the standard procedure described in this section. The C-terminus of human Tuba (amino acids 1,288–1,552) was amplified by PCR and subcloned in the pGEX4T-2 vector (GE Healthcare). The fusion protein was purified by using a GSTrap column (GE Healthcare) according to the manufacturer's protocol. BDF-1 mice (CLEA Japan) were immunized at 4-wk intervals by the i.p. injection of 15 μg per mouse of GST–human Tuba C terminus emulsified with RIBI adjuvant. 5 d after the final immunization, the splenocytes were recovered and fused with P3-X63-Ag-U1 myeloma cells. Culture supernatants were screened by immunofluorescence and Western blotting for their reactivity to Tuba-GFP–stable transfectants, and positive wells were cloned by limited dilution.

The following primary antibodies were used: rabbit polyclonal antibody against α-catenin (C-2081; Sigma-Aldrich), rabbit polyclonal antibody against ZO-1 (61–7,300; Invitrogen), mouse mAb T8-754 specific for ZO-1 (a gift from S. Tsukita; Itoh et al., 1991), rabbit polyclonal antibody against ZO-2 (H-110; Santa Cruz Biotechnology, Inc.), rabbit polyclonal antibody against l-afadin (Sigma-Aldrich), mouse mAb 5H10 against β-catenin (a gift from M.J. Wheelock, University of Nebraska, Omaha, NE; Johnson et al., 1993), mouse mAb HECD-1 specific for human E-cadherin (Shimoyama et al., 1989), mouse mAb against p120-catenin (BD Biosciences), mouse mAb against Cdc42 (BD Biosciences), rabbit polyclonal antibody against N-WASP (H-100; Santa Cruz Biotechnology, Inc.), mouse mAb against MLCs (Sigma-Aldrich), mouse mAb specific for phospho-MLC 2 (Ser19; Cell Signaling Technology), rabbit polyclonal antibody against IQGAP1 (H-109; Santa Cruz Biotechnology, Inc.), mouse mAb DM1A against α-tubulin (Sigma-Aldrich), mouse mAb AC-15 against β-actin (Sigma-Aldrich), rabbit polyclonal antibody reactive with myosin IIA (Sigma-Aldrich), rabbit polyclonal antibody against myosin IIB (Sigma-Aldrich), mouse mAb M2 against Flag (Sigma-Aldrich), rabbit polyclonal antibody specific for Flag (Sigma-Aldrich), rabbit polyclonal antibody against myc (for immunofluorescence; Santa Cruz Biotechnology, Inc.), rabbit polyclonal antibody against myc (for immunoprecipitation; Sigma-Aldrich), mouse mAb 16B12 reactive with HA (CRP), and rabbit polyclonal antibody against HA (Millipore). The following secondary antibodies were used: goat Alexa Fluor 488/594–conjugated anti–mouse or anti–rabbit IgG (Invitrogen) and sheep HRP-conjugated anti–mouse or anti–rabbit IgG (GE Healthcare). F-actin was visualized by using Alexa Fluor 488–conjugated phalloidin (Invitrogen).

Immunofluorescence staining

For staining Tuba, ZO-1, ZO-2, and l-afadin, cells were fixed with 100% methanol at −20°C for 20 min. For staining Cdc42, cells were fixed in 10% TCA at 4°C for 15 min, and permeabilized with 0.2% Triton X-100 for 15 min at RT (Hayashi et al., 1999). Otherwise, cells were fixed with 4% PFA for 20 min or 1.25% PFA for 5 min (for phospho-S19-MLC) by directly adding a 1/4 or 1/16 volume of prewarmed 20% PFA/HBSS to the medium, and permeabilized with 0.1% Triton X-100 for 15 min. Blocking was done by incubating the fixed cells with 5% skim milk in TBS for 10 min at RT. After the antibodies had been diluted with the blocking solution, the cells were incubated at RT for 1 h with the primary antibody, and then for 30 min with the secondary antibody. Samples were mounted in FluorSave (Calbiochem), and imaged by use of a laser scanning confocal microscope (LSM510) mounted on an inverted microscope (Axiovert 100M), using Plan-Neofluar 40×/1.30 NA and Plan-Apochromat 63×/1.40 NA objectives (all Carl Zeiss MicroImaging, Inc.). All images were processed by use of Photoshop (Adobe) software.

Quantification of immunofluorescent signal intensity was done by Scion Image (Scion Corp.). In brief, the junctional regions were manually encircled (see Fig. 4 B for example), and the signal density of each region was measured. The measurement of linearity index was done by LSM 5 Image Browser (Carl Zeiss MicroImaging, Inc.). All statistical analysis was performed by using Excel (Microsoft).

Biochemical assays

For immunoprecipitation, the cells were lysed in lysis buffer (50 mM Tris-HCl, pH 7.5, containing 150 mM NaCl, 0.5% NP-40 or Triton X-100, 1 mM EDTA, and 10% glycerol); NP-40 was used in the myc-N-WASP immunoprecipitation experiments. Lysates were precleared with protein G–Sepharose 4FF beads (GE Healthcare) and incubated with anti-myc polyclonal antibody or anti-HA mAb for 1 h, followed by incubation with protein G–Sepharose beads for 1 h. The beads were subsequently washed three times in the lysis buffer.

For Cdc42 pull-down assays, cells were lysed in HS-buffer (20 mM Tris-HCl, pH 7.4, containing 500 mM NaCl, 5 mM $MgCl_2$, and 1% Triton X-100). 10 μg of GST-PAK CRIB domain (a gift from S. Narumiya) was added to the lysate. After 1 h incubation, the lysate was incubated for another 1 h with glutathione–Sepharose 4B beads (GE Healthcare). The beads were subsequently washed three times in HS buffer.

For the Triton X-100 solubility experiments, cells were lysed in lysis buffer (50 mM Tris-HCl, pH 7.5, containing 150 mM NaCl, and 0.5% Triton X-100), and incubated for 30 min on ice. Lysates were centrifuged at 17,000 *g* for 10 min, and the supernatants were recovered (soluble fraction). The remaining pellet was resuspended to Laemmli sample buffer (insoluble fraction).

All samples were eluted by boiling them in the Laemmli sample buffer, resolved by SDS-PAGE using 10–20% gradient gels (Daiichi Pure Chemicals) for MLC, phospho-S19-MLC, and Cdc42, and using 7.5% gel for others, and transferred to nitrocellulose membrane. Blocking was done using 5% skim milk in TBS. Primary and secondary antibodies were diluted in either the blocking solution or Can Get Signal (TOYOBO), and the membranes were incubated for 1 h with each. Membranes were washed with 0.05% Tween-20 in TBS three times after each antibody incubation, and signals were detected by use of the ECL-plus system (GE Healthcare).

Online supplemental material

Fig. S1 shows that Tuba interacts with ZO-2, but not with ZO-3. Fig. S2 shows the effects of ZO-1 knockdown on junction morphology and myosin localization in comparison with Tuba depletion. Fig. S3 shows that the DH domain of Tuba preferentially activates Cdc42 in vitro. Fig. S4 shows the effects of N-WASP expression on Tuba-RNAi cells. Online supplemental material is available at http://www.jcb.org/cgi/content/full/jcb.200605012/DC1.

We thank S. Yonemura, S. Narumiya, H. Bito, T. Takenawa, M.J. Wheelock, and S. Tsukita for reagents; M. Furuse, and Y. Takai for valuable suggestions; M. Negishi and T. Tanoue for critical reading of the manuscript; and H. Ishigami, M. Harata, M. Uemura, and C. Yoshii for technical assistance.

This work was supported by a grant (to M. Takeichi) from the program Grants-in-Aid for Specially Promoted Research of the Ministry of Education, Science, Sports, and Culture of Japan.

Submitted: 2 May 2006
Accepted: 6 September 2006

References

Amano, M., M. Ito, K. Kimura, Y. Fukata, K. Chihara, T. Nakano, Y. Matsuura, and K. Kaibuchi. 1996. Phosphorylation and activation of myosin by Rho-associated kinase (Rho-kinase). *J. Biol. Chem.* 271:20246–20249.

Ando-Akatsuka, Y., S. Yonemura, M. Itoh, M. Furuse, and S. Tsukita. 1999. Differential behavior of E-cadherin and occludin in their colocalization with ZO-1 during the establishment of epithelial cell polarity. *J. Cell. Physiol.* 179:115–125.

Benais-Pont, G., A. Punn, C. Flores-Maldonado, J. Eckert, G. Raposo, T.P. Fleming, M. Cereijido, M.S. Balda, and K. Matter. 2003. Identification of a tight junction–associated guanine nucleotide exchange factor that activates Rho and regulates paracellular permeability. *J. Cell Biol.* 160:729–740.

Blanchoin, L., K.J. Amann, H.N. Higgs, J.B. Marchand, D.A. Kaiser, and T.D. Pollard. 2000. Direct observation of dendritic actin filament networks nucleated by Arp2/3 complex and WASP/Scar proteins. *Nature*. 404:1007–1011.

Bokoch, G.M., B.P. Bohl, and T.H. Chuang. 1994. Guanine nucleotide exchange regulates membrane translocation of Rac/Rho GTP-binding proteins. *J. Biol. Chem.* 269:31674–31679.

Braga, V.M., and A.S. Yap. 2005. The challenges of abundance: epithelial junctions and small GTPase signalling. *Curr. Opin. Cell Biol.* 17:466–474.

Brummelkamp, T.R., R. Bernards, and R. Agami. 2002. A system for stable expression of short interfering RNAs in mammalian cells. *Science*. 296:550–553.

Chen, X., and I.G. Macara. 2005. Par-3 controls tight junction assembly through the Rac exchange factor Tiam1. *Nat. Cell Biol.* 7:262–269.

Drees, F., S. Pokutta, S. Yamada, W.J. Nelson, and W.I. Weis. 2005. Alpha-catenin is a molecular switch that binds E-cadherin-beta-catenin and regulates actin-filament assembly. *Cell*. 123:903–915.

Etienne-Manneville, S., and A. Hall. 2002. Rho GTPases in cell biology. *Nature*. 420:629–635.

Farquhar, M.G., and G.E. Palade. 1963. Junctional complexes in various epithelia. *J. Cell Biol.* 17:375–412.

Fukata, M., and K. Kaibuchi. 2001. Rho-family GTPases in cadherin-mediated cell-cell adhesion. *Nat. Rev. Mol. Cell Biol.* 2:887–897.

Fukuhara, T., K. Shimizu, T. Kawakatsu, T. Fukuyama, Y. Minami, T. Honda, T. Hoshino, T. Yamada, H. Ogita, M. Okada, and Y. Takai. 2004. Activation of Cdc42 by trans interactions of the cell adhesion molecules nectins through c-Src and Cdc42-GEF FRG. *J. Cell Biol.* 166:393–405.

Hart, M.J., A. Eva, D. Zangrilli, S.A. Aaronson, T. Evans, R.A. Cerione, and Y. Zheng. 1994. Cellular transformation and guanine nucleotide exchange activity are catalyzed by a common domain on the dbl oncogene product. *J. Biol. Chem.* 269:62–65.

Hayashi, K., S. Yonemura, T. Matsui, and S. Tsukita. 1999. Immunofluorescence detection of ezrin/radixin/moesin (ERM) proteins with their carboxyl-terminal threonine phosphorylated in cultured cells and tissues. *J. Cell Sci.* 112:1149–1158.

Hayashi, T., and R.W. Carthew. 2004. Surface mechanics mediate pattern formation in the developing retina. *Nature*. 431:647–652.

Hordijk, P.L., J.P. ten Klooster, R.A. van der Kammen, F. Michiels, L.C. Oomen, and J.G. Collard. 1997. Inhibition of invasion of epithelial cells by Tiam1-Rac signaling. *Science*. 278:1464–1466.

Itoh, M., S. Yonemura, A. Nagafuchi, S. Tsukita, and S. Tsukita. 1991. A 220-kD undercoat-constitutive protein: its specific localization at cadherin-based cell–cell adhesion sites. *J. Cell Biol.* 115:1449–1462.

Ivanov, A.I., D. Hunt, M. Utech, A. Nusrat, and C.A. Parkos. 2005. Differential roles for actin polymerization and a myosin II motor in assembly of the epithelial apical junctional complex. *Mol. Biol. Cell*. 16:2636–2650.

Johnson, K.R., J.E. Lewis, D. Li, J. Wahl, A.P. Soler, K.A. Knudsen, and M.J. Wheelock. 1993. P- and E-cadherin are in separate complexes in cells expressing both cadherins. *Exp. Cell Res.* 207:252–260.

Kawasaki, Y., R. Sato, and T. Akiyama. 2003. Mutated APC and Asef are involved in the migration of colorectal tumour cells. *Nat. Cell Biol.* 5:211–215.

Kim, S.H., Z. Li, and D.B. Sacks. 2000. E-cadherin-mediated cell-cell attachment activates Cdc42. *J. Biol. Chem.* 275:36999–37005.

Kodama, A., K. Takaishi, K. Nakano, H. Nishioka, and Y. Takai. 1999. Involvement of Cdc42 small G protein in cell-cell adhesion, migration and morphology of MDCK cells. *Oncogene*. 18:3996–4006.

Kovacs, E.M., M. Goodwin, R.G. Ali, A.D. Paterson, and A.S. Yap. 2002. Cadherin-directed actin assembly: E-cadherin physically associates with the Arp2/3 complex to direct actin assembly in nascent adhesive contacts. *Curr. Biol.* 12:379–382.

Kovacs, E.M., R.S. Makar, and F.B. Gertler. 2006. Tuba stimulates intracellular N-WASP-dependent actin assembly. *J. Cell Sci.* 119:2715–2726.

Kuroda, S., M. Fukata, M. Nakagawa, K. Fujii, T. Nakamura, T. Ookubo, I. Izawa, T. Nagase, N. Nomura, H. Tani, et al. 1998. Role of IQGAP1, a target of the small GTPases Cdc42 and Rac1, in regulation of E-cadherin-mediated cell-cell adhesion. *Science*. 281:832–835.

Malliri, A., S. van Es, S. Huveneers, and J.G. Collard. 2004. The Rac exchange factor Tiam1 is required for the establishment and maintenance of cadherin-based adhesions. *J. Biol. Chem.* 279:30092–30098.

Mandai, K., H. Nakanishi, A. Satoh, H. Obaishi, M. Wada, H. Nishioka, M. Itoh, A. Mizoguchi, T. Aoki, T. Fujimoto, et al. 1997. Afadin: a novel actin filament–binding protein with one PDZ domain localized at cadherin-based cell-to-cell adherens junction. *J. Cell Biol.* 139:517–528.

McNeil, E., C.T. Capaldo, and I.G. Macara. 2006. Zonula occludens-1 function in the assembly of tight junctions in Madin-Darby canine kidney epithelial cells. *Mol. Biol. Cell*. 17:1922–1932.

Mertens, A.E., T.P. Rygiel, C. Olivo, R. van der Kammen, and J.G. Collard. 2005. The Rac activator Tiam1 controls tight junction biogenesis in keratinocytes through binding to and activation of the Par polarity complex. *J. Cell Biol.* 170:1029–1037.

Noren, N.K., C.M. Niessen, B.M. Gumbiner, and K. Burridge. 2001. Cadherin engagement regulates Rho family GTPases. *J. Biol. Chem.* 276:33305–33308.

Noritake, J., M. Fukata, K. Sato, M. Nakagawa, T. Watanabe, N. Izumi, S. Wang, Y. Fukata, and K. Kaibuchi. 2004. Positive role of IQGAP1, an effector of Rac1, in actin-meshwork formation at sites of cell-cell contact. *Mol. Biol. Cell*. 15:1065–1076.

Petersen, N.O., W.B. McConnaughey, and E.L. Elson. 1982. Dependence of locally measured cellular deformability on position on the cell, temperature, and cytochalasin B. *Proc. Natl. Acad. Sci. USA*. 79:5327–5331.

Rajasekaran, A.K., M. Hojo, T. Huima, and E. Rodriguez-Boulan. 1996. Catenins and zonula occludens-1 form a complex during early stages in the assembly of tight junctions. *J. Cell Biol.* 132:451–463.

Rimm, D.L., E.R. Koslov, P. Kebriaei, C.D. Cianci, and J.S. Morrow. 1995. Alpha 1(E)-catenin is an actin-binding and -bundling protein mediating the attachment of F-actin to the membrane adhesion complex. *Proc. Natl. Acad. Sci. USA*. 92:8813–8817.

Rohatgi, R., L. Ma, H. Miki, M. Lopez, T. Kirchhausen, T. Takenawa, and M.W. Kirschner. 1999. The interaction between N-WASP and the Arp2/3 complex links Cdc42-dependent signals to actin assembly. *Cell*. 97:221–231.

Salazar, M.A., A.V. Kwiatkowski, L. Pellegrini, G. Cestra, M.H. Butler, K.L. Rossman, D.M. Serna, J. Sondek, F.B. Gertler, and P. De Camilli. 2003. Tuba, a novel protein containing bin/amphiphysin/Rvs and Dbl homology domains, links dynamin to regulation of the actin cytoskeleton. *J. Biol. Chem.* 278:49031–49043.

Schmidt, A., and A. Hall. 2002. Guanine nucleotide exchange factors for Rho GTPases: turning on the switch. *Genes Dev.* 16:1587–1609.

Shimoyama, Y., S. Hirohashi, S. Hirano, M. Noguchi, Y. Shimosato, M. Takeichi, and O. Abe. 1989. Cadherin cell-adhesion molecules in human epithelial tissues and carcinomas. *Cancer Res.* 49:2128–2133.

Thompson, D.W. 1917. On Growth and Form. Cambridge University Press, Cambridge, England. 793 pp.

Uehata, M., T. Ishizaki, H. Satoh, T. Ono, T. Kawahara, T. Morishita, H. Tamakawa, K. Yamagami, J. Inui, M. Maekawa, and S. Narumiya. 1997. Calcium sensitization of smooth muscle mediated by a Rho-associated protein kinase in hypertension. *Nature*. 389:990–994.

Umeda, K., T. Matsui, M. Nakayama, K. Furuse, H. Sasaki, M. Furuse, and S. Tsukita. 2004. Establishment and characterization of cultured epithelial cells lacking expression of ZO-1. *J. Biol. Chem.* 279:44785–44794.

Verma, S., A.M. Shewan, J.A. Scott, F.M. Helwani, N.R. den Elzen, H. Miki, T. Takenawa, and A.S. Yap. 2004. Arp2/3 activity is necessary for efficient formation of E-cadherin adhesive contacts. *J. Biol. Chem.* 279:34062–34070.

Watabe-Uchida, M., N. Uchida, Y. Imamura, A. Nagafuchi, K. Fujimoto, T. Uemura, S. Vermeulen, F. van Roy, E.D. Adamson, and M. Takeichi. 1998. α-Catenin–vinculin interaction functions to organize the apical junctional complex in epithelial cells. *J. Cell Biol.* 142:847–857.

Yamada, S., S. Pokutta, F. Drees, W.I. Weis, and W.J. Nelson. 2005. Deconstructing the cadherin-catenin-actin complex. *Cell*. 123:889–901.